

Review Article

Yoshiki Nakata*

Interference laser processing

DOI 10.1515/aot-2015-0060

Received December 9, 2015; accepted January 8, 2016; previously published online February 4, 2016

Abstract: The most important component of quantum optics is laser interference. Interference patterns are formed by splitting a coherent beam into multiple beams and correlating them. This study introduces a variety of beam correlators and discusses their characteristics. Beam correlator basics such as interference region in terms of pulse width, group delay dispersion effects on pulse width, optical delay adjustment, and interference pattern simulation are explained. A discussion of the history of interference processing begins with the method in 1967 and continues through the advancement of shorter wavelengths and pulse widths. The recent techniques of solid-liquid-solid for 3D nanofabrication, duplicated structures with laser-induced periodic surface structure, processing inside transparent materials, and 2D and 3D periodic structures fabricated by photo-sensitization are also presented.

Keywords: beam correlator; interference; laser processing; nanostructure; periodic structure; simulation of interference pattern.

1 Introduction

Temporal and spatial coherence of laser beams enable the formation of a periodic distribution of electromagnetic energy, which is represented by an interference pattern. Extensive attempts have been made to transcribing interference pattern on or within materials since the invention of the laser. Direct ablation of the material surface by an interfering nanosecond (ns) laser was tested in 1967 [1]. The quality was poor because of the low spatial resolution due to the thermal detriment. However, spatial resolution

was improved using a photo-dissociative polymer [2]. More recently, ultrashort pulse lasers such as femtosecond (fs) and picosecond (ps) lasers have enabled material processing at nanoscale resolution with only a small thermal detriment [3–5]. They have also been applied to interfering laser processing and enable fabrication of a variety of periodic structures on the surface of and within materials.

This article introduces various laser beam correlators and discusses their characteristics. Elongation of pulse width by group delay dispersion (GDD) and correlation of an ultrashort pulse beam are explained for practical experiments with ultrashort pulse lasers. Control of interference patterns through beam number, phase shift, and amplitude variation among beams is numerically simulated. This level of control enables the fabrication of large amounts of lattice units in a single process. The results of early experiments with interfering ns lasers are introduced. Fabrication of lattice nanostructures with interfering fs lasers is described next using different targets such as metal thin films and bulks. Applications of interfering laser processing is also discussed, e.g. nanofabrication of photo-sensitive resin and the fabrication of a distributed-feedback color-center laser.

2 Laser beam correlators

2.1 Various laser beam correlators used in interference processing

The Mach-Zehnder interferometer shown in Figure 1A was first conceived in 1891. It observes the phase variation that results from an object inserted in the beam path. Lenses may also be inserted along the two resulting paths to increase fluence for material processing [6]. The number of beam splitters (BSs) and mirrors increases with the number of beams, and optical delay is critical in the case of an ultrashort pulse laser. The length of a pulsed laser is $l=c\Delta t/n$, where c is the speed of light in vacuum, Δt is the pulse width, and n is the refractive index. For example, $l=30\ \mu\text{m}$ with $\Delta t=100\ \text{fs}$, so the delay path length must be set in this spatial resolution. The interference region

*Corresponding author: Yoshiki Nakata, Institute of Laser Engineering, Osaka University, 2-6 Yamadaoka, Suita, Osaka 565-0871, Japan, e-mail: nakata-y@ile.osaka-u.ac.jp

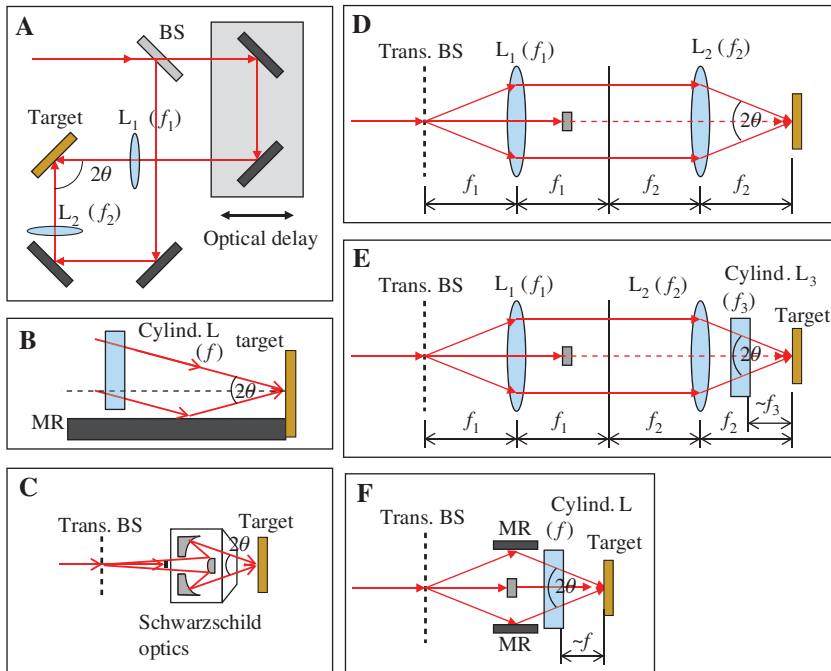


Figure 1: Beam correlators. (A) Mach-Zehnder, (B) Lloyd's mirror, (C) transmission BS with Schwarzschild optics, (D) transmission BS and demagnification system ($4F$ correlator if $f_1=f_2$), (E) cylindrical lens added to (D), and (F) Talbot interferometer.

is also narrow and will be explained in Subsection 2.3. Lloyd's mirror is another scheme used historically that has a simple setup as shown in Figure 1B. A beam is partially separated, and a portion is reflected. This configuration can be extended to use with a three-beam correlation [7], but not suitable for an ultrashort pulse laser because the optical delay cannot be adjusted.

Schwarzschild optic (Figure 1C) is a focusing or imaging optics system with no chromatic aberration or pulse elongation from dispersion. In this scheme, a beam is split by a transmission BS, and first-order diffracted beams correlate on a target surface via two reflections. However, beam diameter and correlation angle are restricted, and the zero-order beam cannot reach the target.

Figure 1D shows a beam correlator composed of a transmission BS and a demagnification system that consists of two convex lenses, L_1 and L_2 . This configuration is also known as a $4F$ (basically $f_1=f_2$) correlator, which is based on the Fourier transform theory. The interference region in this scheme expands to the entire beam diameter, as explained in Subsection 2.3. In addition, this simple scheme can be applied to any number of beams split by a special transmission BS. A cylindrical lens (L_3) inserted between the second lens (L_2) and the target allows dotted line formation or increased fluence (Figure 1E). Figure 1F shows a Talbot interferometer that can be used for a narrow bandwidth laser.

2.2 Adjustment of optical delay to superimpose ultrashort pulse laser beams

The thickness of a plane wave is $l=c\Delta t/n$, which is tens of μm for a typical fs laser system. Optical delay must be adjusted to superimpose multiple beams and correlate ultrashort pulse laser beams with a Mach-Zehnder beam correlator. An intensity autocorrelator, wherein a nonlinear crystal is inserted in the beam collision area, is useful in this case. Adjustment of the phase-matching angle and optical delay to maximize the second-harmonic generation optimizes superimposition of thin plane waves. If the peak power density is high enough, the third-harmonic generation in air is more sensitive, and the setup is simpler [8]. However, optical delay is automatically adjusted in the case of beam correlators that use a transmission BS and a demagnification system or Schwarzschild optics with a coaxial alignment.

2.3 Correlation width as a function of pulse width

Restriction of the correlation region for an ultrashort pulse laser is performed as follows. Mach-Zehnder interferometers form an angle between plane waves, as seen

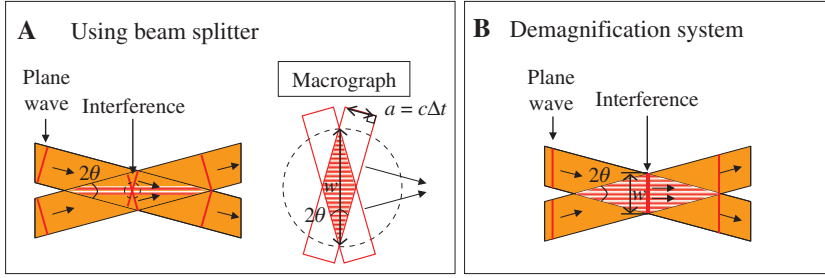


Figure 2: Width of overlapping region (A) in a correlator using a reflecting BS and (B) using a transmission BS and a demagnification system.

in Figure 2A. The width of the interference pattern in this case is restricted to $w=c\Delta t/\sin(\theta)$, as illustrated by the macrograph. For example, $w=173\ \mu\text{m}$ with $\Delta t=100\ \text{fs}$ and $\theta=10^\circ$, and the interference pattern occurs only inside this width. However, Maznev et al. showed that the Figure 1D scheme achieves correlation of a fs laser over the entire beam diameter, as seen in Figure 2B [9]. Their demonstration successfully generated a second-harmonic wave of a 30-fs laser with a full beam diameter (4 mm) through correlation in a nonlinear crystal. When processing material with the scheme in Figure 1E, the periodic hole structure was fabricated over the entire beam size of $w=6.0\ \text{mm}$ using a 90-fs pulsed laser [10]. This is much larger than the restriction obtained with inclined beams.

2.4 Elongation of pulse width as a function of glass thickness

The effect of dispersion should be considered for all setups. The pulse width elongation of a mode-locked laser can be expressed as follows:

$$\Delta t_{\text{out}} = \frac{\sqrt{\Delta t_{\text{in}}^4 + 16(\ln 2)^2 \phi_2}}{\Delta t_{\text{in}}}, \quad (1)$$

where ϕ_2 is the GDD parameter of the medium. GDD is proportional to the group velocity dispersion (GVD) that changes according to medium and wavelength. Their relationship is as follows:

$$\phi_2 = k_2(w)L, \quad (2)$$

where L is the medium thickness. The relationship between input and output pulse width after transmission of three representative medium is shown in Figure 3. A GVD of 800 nm is used in the calculation of all glass. No pulse elongation occurs in the case of ns and ps lasers, although it seems to appear under 150 fs. The GDD effect is more apparent in SF10 that has a larger GVD compared with

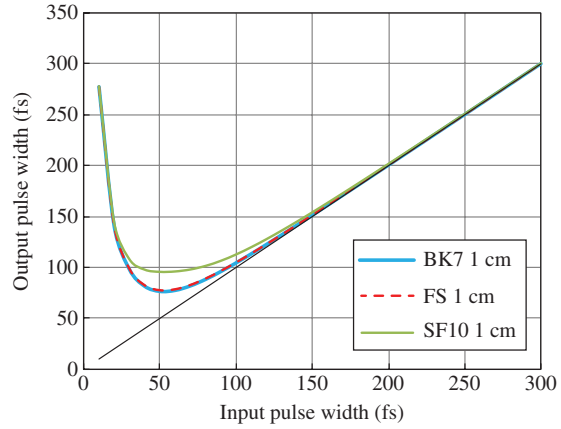


Figure 3: Elongation of pulse width by GDD calculated for BK7, fused silica, and SF10 with 1 cm thickness.

the other glasses. SF10 is used frequently as a medium for achromatic lenses, which is useful to lessen the effect of chromatic aberration. The GDD effect should be considered when designing a beam correlator with a fs laser.

3 Simulation of interference patterns

Laser processing by interference patterns usually involves a beam split into beams of equal intensity. However, the interference pattern changes as a function of the number of beams, phase shift, and amplitude variation among the beams [11–14]. Unlike pattern control by a spatial light modulator, thousands of structures in the same design can be fabricated in a single process. Numerically simulated interference patterns are achieved as follows.

The electric field of each beam can be expressed as

$$\begin{aligned} E_n(E_{n0}, x, y, z, k_n, \theta_n, \phi_n, \alpha_n, \omega_n, t) \\ = E_{n0} \cos\{k_n(-x \sin\theta_n \cos\phi_n - y \sin\theta_n \sin\phi_n \\ + z \cos\theta_n) - \omega_n t + \alpha_n\}, \end{aligned} \quad (3)$$

where n is the number of beams, E_{n0} is the amplitude of a beam, k_n is the wavenumber, θ_n is the polar angle, ϕ_n is the azimuthal angle, α_n is the phase shift added to a beam, and $\omega_n = 2\pi c/\lambda_n$ is the angular velocity. The intensity distribution of multiple correlated beams can be explained as

$$I(E_{n0}, x, y, z, k_n, \theta_n, \phi_n, \alpha_n, \omega_n) \propto \int \left| \sum_{n=1,2,\dots}^N E_n(E_{n0}, x, y, z, k_n, \theta_n, \phi_n, \alpha_n, \omega_n, t) \right|^2 dt. \quad (4)$$

The interference pattern can be simulated by the integration of the intensity distribution for a cycle, $\Delta t = \lambda_n/c$.

Figure 4 represents the scheme for four- and six-beam correlations on a target surface. The following simulation assumes $\lambda_n = 785$ nm, $\theta_n = 20^\circ$, and $\Delta\phi_n = 2\pi/n$.

3.1 Beams with equivalent azimuthal angles

The experimental setup in Figure 1D permits the number of correlated beams to be easily controlled by changing

the transmission BS. The interference patterns on the x-y plane for different amounts of beams of equal azimuthal angle difference are shown in Figure 5 [15]. No phase shift or amplitude variation was assumed. The brightness of each image was normalized to its peak intensity.

The grating pattern for a two-beam correlation is seen in Figure 5A. The peaks from three and four beams have triangular and square lattices (Figure 5B and C), respectively. A similar pattern with a lattice $\sqrt{3}$ times longer appears from six beams (Figure 5E). Meanwhile, symmetric point patterns appear in the other examples.

3.2 2D interference patterns from four and six beams with phase shift and amplitude variation

The interference patterns from four [12] and six [11] beams with phase shift and amplitude variation are shown.

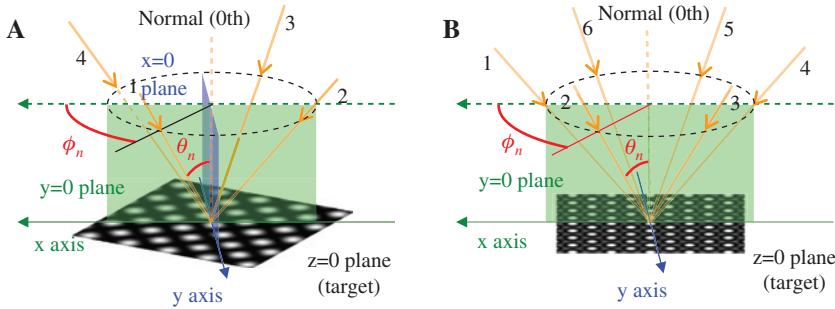


Figure 4: Scheme for multiple beam correlation of (A) four beams, (B) six beams.

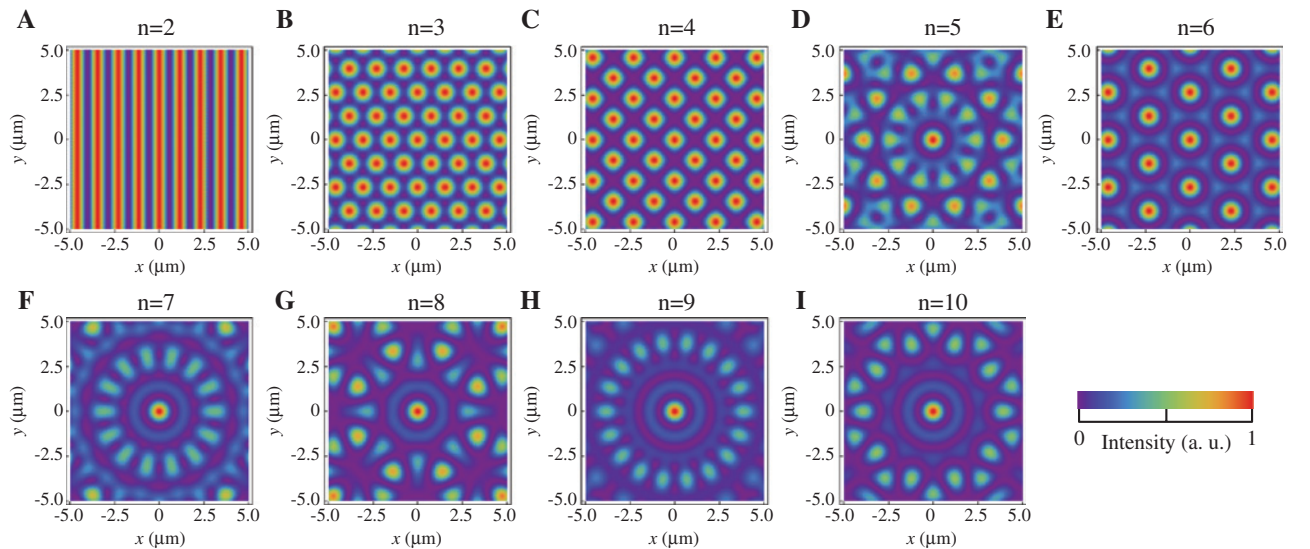


Figure 5: Interference patterns for various beams of equal azimuthal angle difference ϕ_n . Reproduced from Ref. [15] with permission. Copyright (2012) SPIE.

They are shown in rainbow scale with the corresponding interference conditions in the diagrams above the patterns. The rule is displayed in the upper left corner of the diagram (Figure 6).

The interference pattern of four beams without phase shift or amplitude variation is shown in Figure 6A with individual spots in a square lattice. Residual peaks appear between the original peaks with a phase shift of $\alpha_1=5\pi/6$ (Figure 6B). The peak density doubles with the phase shift of $\alpha_1=\pi$ (Figure 6C). The shape of the spots can be controlled simultaneously by phase shift and amplitude variation. Figure 6D displays an island in the lattice, and E is the negative pattern of D.

The interference pattern of six beams without phase shift or amplitude variation shows spots in a triangular lattice (Figure 6F). The phase shift $\alpha_1=\pi$ is represented by islands in a square matrix (Figure 6H). The garter stitch (Figure 6I) and split-ring resonator (SRR) (Figure 6J) characteristics appear with phase shift and amplitude variation. SRR pattern is useful for the fabrication of meta-materials that have nonlinearity.

A variety of interference patterns from four and six counteracting beams have been summarized [11, 12]. In addition, a periodic structure appears over the z direction by adding the zero-order beam in the Figure 1D configuration [16, 17]. This scheme is useful for the fabrication of 3D

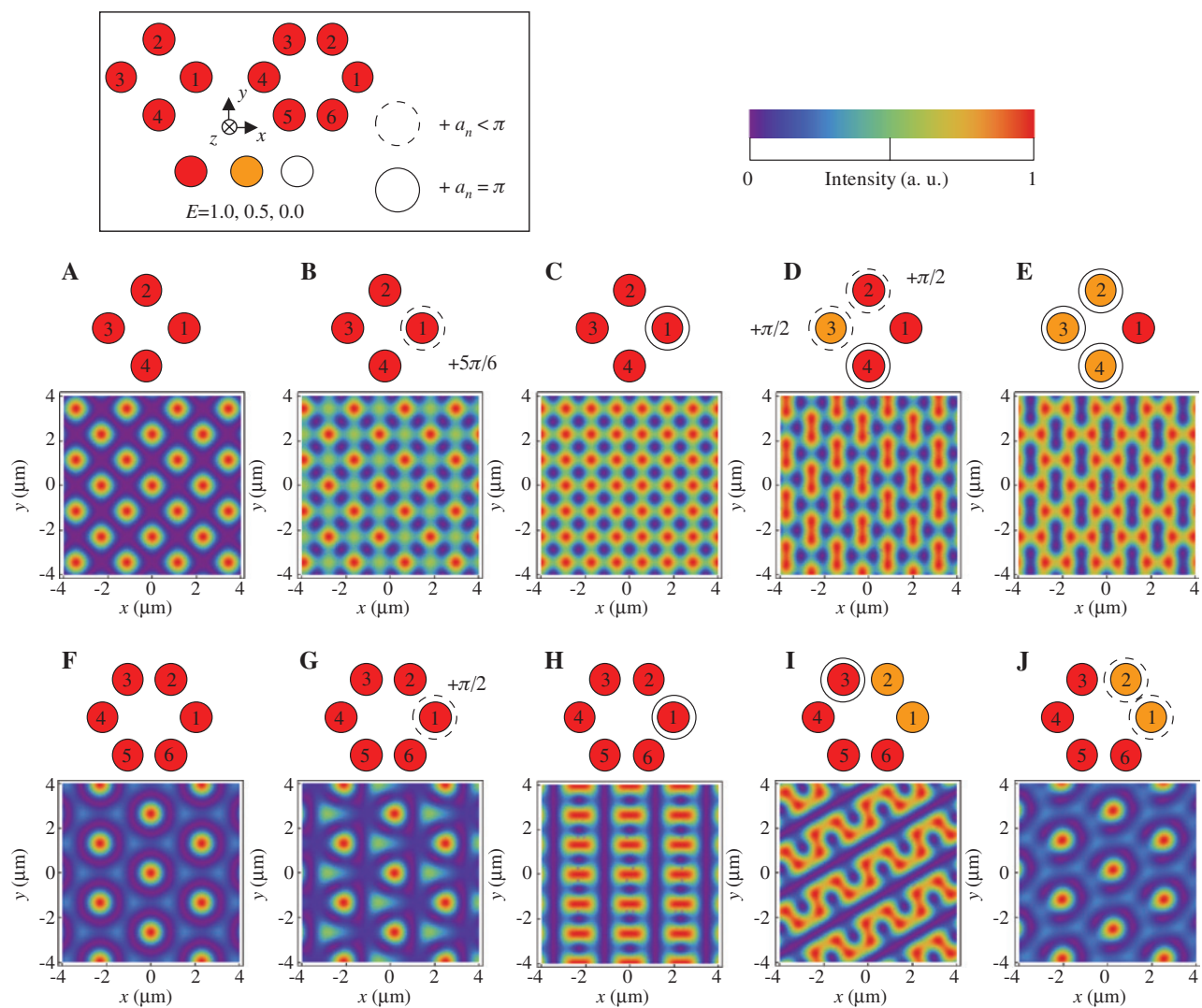


Figure 6: Interference patterns from four and six beams [11, 12]. Diagrams above each interference pattern portray the phase shift and amplitude variation, and the rule is displayed in the upper left corner. Reproduced from Ref. [12] with permission. Copyright (2012) Springer. Reproduced from Ref. [11] with permission. Copyright (2012) OSA.

photonic structures by the photo-sensitization of resin, as described in Section 7.

4 Interfering ns laser processing

Interfering ns laser processing was examined in 1967 soon after the invention of the laser [1]. Figure 7 shows an electrolytic copper target irradiated by a ‘giant pulse’ from a ruby laser. The pulse width was 30 ns, and a grating with $L=2.42\ \mu\text{m}$ was fabricated. The thermal conduction during the pulse width resulted in a processing threshold higher than $10^9\ \text{W}/\text{cm}^2$ and leveling of the periodic energy induction by the interference pattern and low processing quality. However, a UV laser can etch polymers via photo-dissociation without thermal damage [3], and a period shorter than 200 nm can be fabricated by the interference pattern of an UV laser [2]. Therefore, the combination of wavelength region and target material is important in situations where long pulse lasers are used.

5 Interfering ps and fs laser processing

High-power ultrashort pulse lasers based on the dye laser-seeded excimer laser were developed in the 1980s. Interfering ps (5 and 50 ps) KrF laser processing of copper with a 364-nm spacing grating via Schwarzschild objectives was performed in 1996 [18]. The processing quality was improved by shortening the pulse width. The Kerr lens mode-locking technique with a Ti:sapphire crystal

became popular in the 1990s for its simplicity and stability. The regeneratively amplified fs pulse used by this technique was applied to interfering laser processing in the Mach-Zehnder interferometry system (Figure 1A). This resulted in a periodic line pattern with $2.5\ \mu\text{m}$ spacing written on crystals such as sapphire and silica (Figure 8A) [8, 19]. Metallic thin films were also processed by a transmission BS with the demagnification system shown in Figure 1E. A 6-mm line of hole structure could be fabricated in a single shot on metallic thin film because of the wide interference region (Figure 8B, Section 2.3), metallic hole array, and grating structures [10, 20].

More than three beams have created a variety of interference patterns. Three beams resulted in circular spots in a triangular lattice with $\Delta\varphi_{1-3}=120^\circ$ [7] and ellipsoidal spots in a square lattice with $\Delta\varphi_{1,2}=90^\circ$ and $\Delta\varphi_3=180^\circ$ [21]. Four beams formed circular spots in a square lattice with $\Delta\varphi_{1-4}=90^\circ$ [21]. A rhombic lattice was also fabricated (the beam number and azimuthal angle were not reported) [22]. Duplicated or designed patterns can be formed by phase shift α_n and amplitude variation among beams [23, 24]. Peak density doubled with $\alpha_{1,3}=0.5\pi$ [13] as in the same pattern with $\alpha_1=\pi$ in Figure 6C, but the position shifted [23]. Six beams resulted in a more complicated structure fabricated with azimuthal angle $\Delta\phi=20^\circ$ and phase shift $\alpha=0.5\pi$ [13].

5.1 Processing thin films and solid-liquid-solid process

The fs laser has been used for its low thermal detriment when processing. However, the thermal process

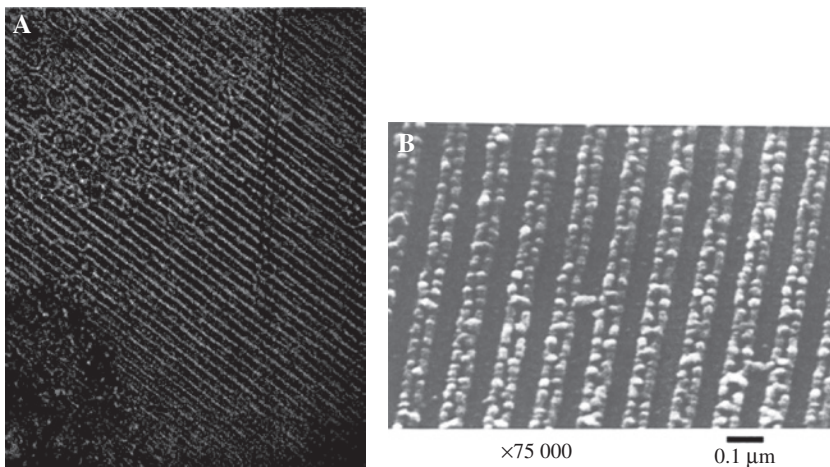


Figure 7: (A) Electrolytic copper target exposed to the interference pattern of a ruby laser (30 ns). Spacing= $2.42\ \mu\text{m}$. Reproduced from Ref. [1] with permission. Copyright (1967) AIP Publishing LLC. (B) Polyimide target exposed to the interference pattern of a KrF laser. Spacing= $167\ \text{nm}$. Reproduced from Ref. [2] with permission. Copyright (1991) AIP Publishing LLC.

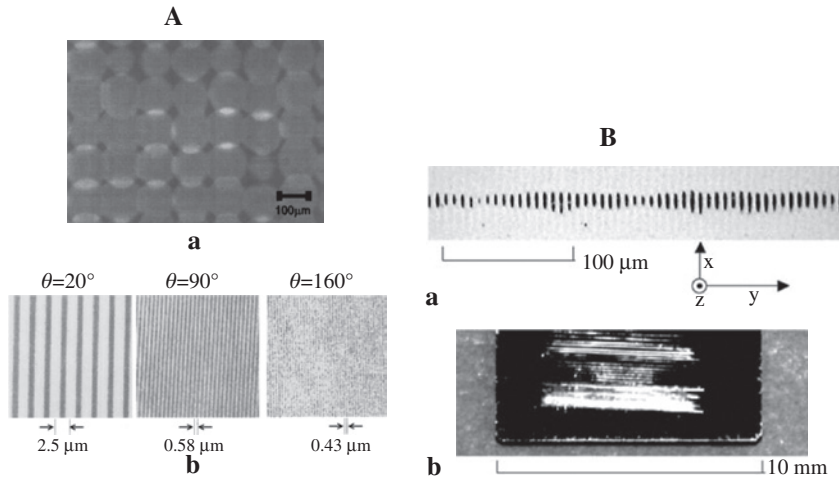


Figure 8: (A) Amorphous silica thin film on *p*-type Si wafer processed by the interference pattern of a Ti:sapphire laser (100 fs). Separation=2.5 μm, 0.58 μm, and 0.43 μm. Reproduced from Ref. [8] with permission. Copyright (2002) AIP Publishing LLC. (B) A 200-nm-thick gold thin film on silica glass processed by the interference pattern of a Ti:sapphire laser (90 fs). Separation=6.25 μm. Reproduced from Ref. [10] with permission. Copyright (2003) Springer.

in a small region of thin film induces prominent motion in the molten layer and allows the fabrication of a high-aspect ratio nanostructure. Figure 10A shows a hollow nanobump, nanodrop, and metallic hole array structure fabricated in a 50-nm-thick gold thin film on a silica substrate by irradiation of the interference pattern of four fs laser beams [21, 25]. The interior of the nanostructure is empty as determined by structure exfoliation and atomic

force microscopy (Figure 9B). The driving force is the vapor pressure and thermal expansion of the thin film [25, 27]. A nanoball far smaller than the wavelength can be formed by surface tension under different conditions [23, 27, 28]. Moreover, a nanowhisker with curvature radius $r=4$ nm, comparable with the size of a multi-wall carbon nanotube, forms by detaching a nanoball (Figure 9C) [26, 28–30]. The process of forming nanostructures via the liquid phase

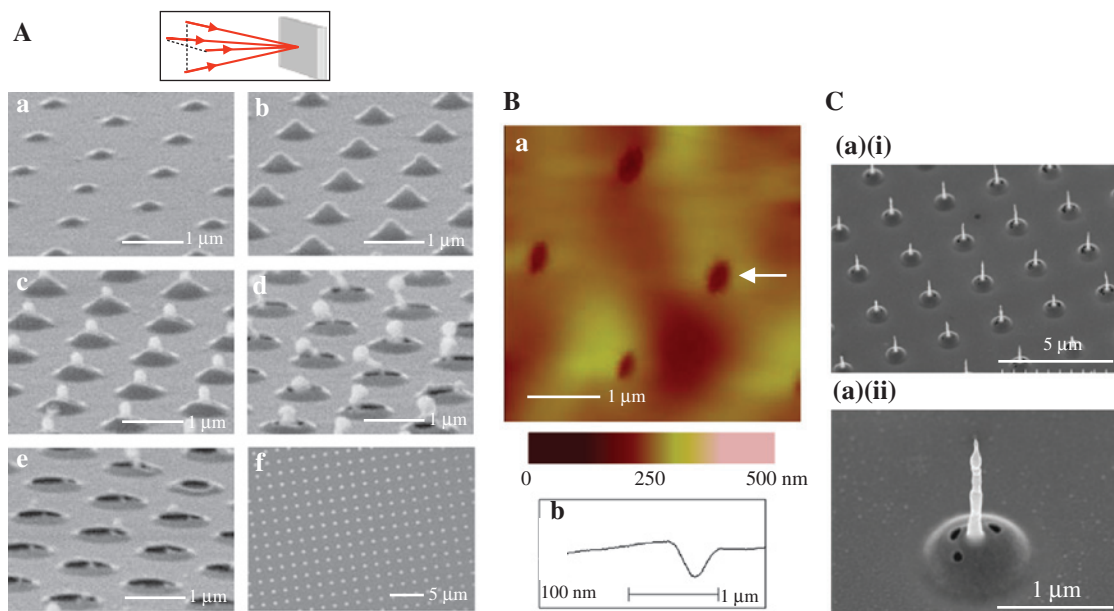


Figure 9: (A) A series of nanostructures in a lattice formed on gold thin film by interfering fs laser processing at different fluences [21, 25]. Reproduced from Ref. [21] with permission. Copyright (2003) The Japan Society of Applied Physics. (B) Morphology of the back of the nanobump in (A) and (C) gold nanowhiskers. Reproduced from Ref. [26] with permission. Copyright (2013) Elsevier.

induced by laser irradiation is referred to as the solid-liquid-solid (SLS) mechanism. This is in contrast to the well-known vapor-liquid-solid method that uses a bottom-up mechanism to process nanostructures [31].

5.2 Duplicated structure with LIPSS

A LIPSS is formed by multiple shots from a laser approximately at the ablation threshold. Application of this phenomenon to interfering laser processing creates a surface structure with a dual period. Figure 10 shows the textured surface of Cr thin film on silica glass irradiated by 50 shots of the interference pattern from two beams at 59 mJ/cm² average fluence. 2D fast Fourier transform (FFT) is very useful for the analysis of the periodicity of nanomaterials with a LIPSS [32]. Figure 10 shows signals in magnified 2D FFT images due to a 1.2- μ m period formed by the interference pattern. However, blur signals indicated by the arrows are due to the LIPSS. The periods were (a) 242 nm and (b) 177 nm, respectively.

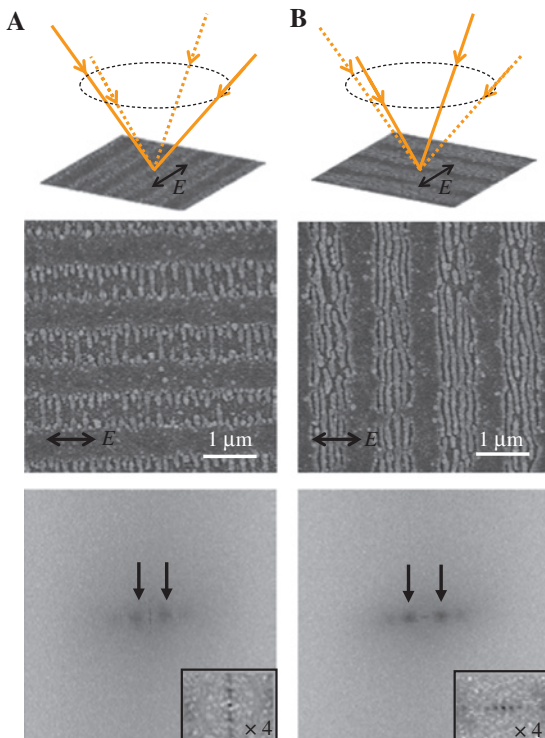


Figure 10: Dual periodic structures of the interference pattern and LIPSS for different polarizations. Upper sketches represent beam correlation and polarization of beams. Lower images are 2D FFT images of each structure. Arrows indicate the most probable period of the LIPSS. Magnified 2D FFT images are also shown. Reproduced from Ref. [32] with permission. Copyright (2010) Springer.

6 Processing inside materials by fs laser

The setups shown in Figure 1A, E, and F can be used to fabricate a periodic structure inside a transparent material. The adaptability of the fs laser to hard materials has permitted the fabrication of a grating with a 2.5- μ m spacing inside the diamond [6] and silica glass [33]. In addition, a distributed-feedback color-center laser was fabricated within a LiF crystal [34]. The line spacing of the grating was 510 nm, and lasing at 710 nm was observed by a 450-nm pumping (Figure 11).

7 Photo-polymerization by interference pattern

This scheme enables fabrication of 2D and 3D lattice patterns from a single exposure process of photo-sensitive

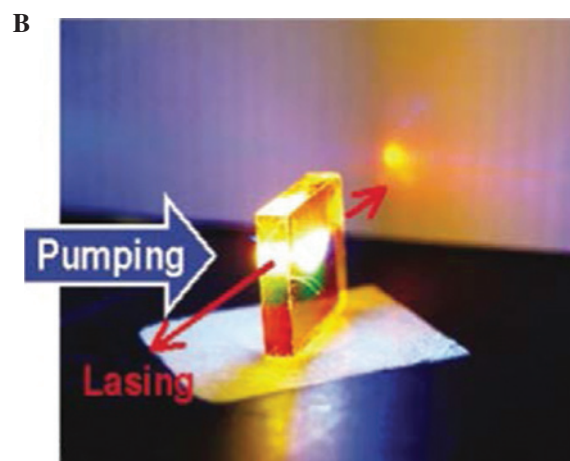
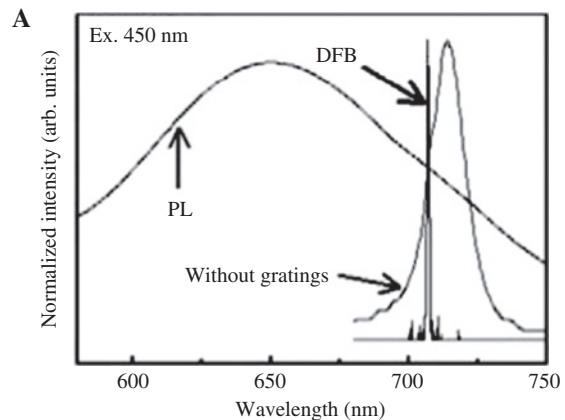


Figure 11: Lasing of a distributed-feedback color-center laser written inside a LiF crystal pumped at 450 nm. Reproduced from Ref. [34] with permission. Copyright (2004) AIP Publishing LLC.

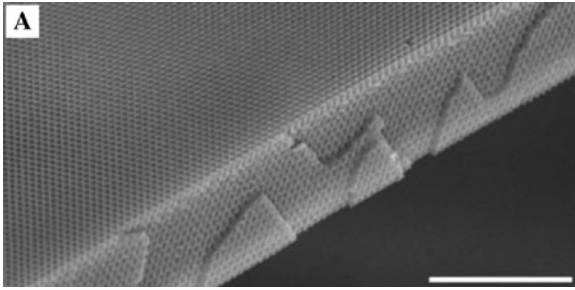


Figure 12: Polymeric photonic crystal generated by exposure of a film containing SU-8. Scale bar is 10 μm . Reproduced from Ref. [16] with permission. Copyright (2000) Nature.

resin. Here, the interference pattern of two beams forms a periodic line pattern applied to the resolution measurement in photolithography. Polymerization occurs and forms a 2D square matrix when using four counteracting beams, as shown in Figure 4A [35]. However, when the 0th beam with $\theta_0=0^\circ$ is added to the three counteracting beams with $\Delta\phi=120^\circ$ (Figure 12) [16] or to four counteracting beams with $\Delta\phi=90^\circ$ [36], a photonic crystal was fabricated successfully.

8 Conclusions

Interfering laser processing techniques are useful for fabricating lattice nanostructures in a single process. These techniques have developed along with the progress of laser technology. Therefore, the variety of structures and new schemes will continue to increase and serve various applications in many scientific and practical fields. Especially, they will be used in nanophotonics, nanoelectronics, and plasmonics.

References

- [1] H. J. Gerritsen, *J. Appl. Phys.* 38, 2054 (1967).
- [2] H. M. Phillips, D. L. Callahan, R. Sauerbrey, G. Szabó and Z. Bor, *Appl. Phys. Lett.* 58, 2761 (1991).
- [3] R. Srinivasan, *Science* 234, 559 (1986).
- [4] S. Kiipter and M. Stuke, *Appl. Phys. B* 44, 199 (1987).
- [5] P. P. Pronko, S. K. Dutta, J. Squier, J. V. Rudd, D. Du, et al. *Opt. Commun.* 114, 106 (1995).
- [6] K. Kawamura, N. S. Arukura, M. Hirano and H. Hosono, *Jpn. J. Appl. Phys.* 39, 767 (2000).
- [7] J. de Boer, N. Geyer, U. Gösele and V. Schmidt, *Opt. Lett.* 34, 1783 (2009).
- [8] K. Kawamura, N. Ito, N. Sarukura, M. Hirano and H. Hosono, *Rev. Sci. Instrum.* 73, 1711 (2002).
- [9] A. A. Maznev, T. F. Crimmins and K. A. Nelson, *Opt. Lett.* 23, 1378 (1998).
- [10] Y. Nakata, T. Okada and M. Maeda, *Appl. Phys. A Mater. Sci. Process.* 77, 399 (2003).
- [11] Y. Nakata, K. Murakawa, K. Sonoda, K. Momoo and N. Miyanaga, *Appl. Opt.* 51, 5004 (2012).
- [12] Y. Nakata, K. Murakawa, K. Sonoda, K. Momoo, N. Miyanaga, et al. *Appl. Phys. A* 112, 191 (2012).
- [13] J. H. Klein-Wiele and P. Simon, *Appl. Phys. Lett.* 83, 4707 (2003).
- [14] T. Kondo, S. Matsuo, S. Juodkakis and H. Misawa, *Appl. Phys. Lett.* 79, 725 (2001).
- [15] K. Momoo, K. Sonoda, Y. Nakata and N. Miyanaga, *Proc. SPIE* 8243, 82431E1-9 (2012).
- [16] M. Campbell, D. N. Sharp, M. T. Harrison, R. G. Denning and A. J. Turberfield, *Nature* 404, 53 (2000).
- [17] T. Kondo, K. Yamasaki, S. Juodkakis, S. Matsuo, V. Mizeikis, et al. *Thin Solid Films* 550, 453–454 (2004).
- [18] P. Simon and J. Ihlemann, *Appl. Phys. A-Materials Sci. Process.* 63, 505 (1996).
- [19] K. Kawamura, T. Ogawa, N. Sarukura, M. Hirano and H. Hosono, *Appl. Phys. B* 71, 119 (2000).
- [20] Y. Nakata, T. Okada and M. Maeda, *Appl. Phys. Lett.* 81, 4239 (2002).
- [21] Y. Nakata, T. Okada and M. Maeda, *Japanese J. Appl. Physics, Part 2 Lett.* 42, L1452 (2003).
- [22] J. Békési, J.-H. Klein-Wiele and P. Simon, *Appl. Phys. A Mater. Sci. Process* 76, 355 (2003).
- [23] Y. Nakata, T. Hiromoto and N. Miyanaga, *Appl. Phys. A Mater. Sci. Process.* 101, 471 (2010).
- [24] Y. Nakata, K. Momoo, T. Hiromoto and N. Miyanaga, *Proc. SPIE* 7920, 79200B1-9 (2011).
- [25] Y. Nakata, Japan Patent Kokai 4322045 (2004).
- [26] Y. Nakata, N. Miyanaga, K. Momoo and T. Hiromoto, *Appl. Surf. Sci.* 274, 27 (2013).
- [27] Y. Nakata, N. Miyanaga and T. Okada, *Appl. Surf. Sci.* 253, 6555 (2007).
- [28] Y. Nakata, K. Tsuchida, N. Miyanaga and H. Furusho, *Appl. Surf. Sci.* 255, 9761 (2009).
- [29] Y. Nakata, N. Miyanaga, K. Momoo and T. Hiromoto, *Jpn. J. Appl. Phys.* 53, 096701 (2014).
- [30] Y. Nakata, K. Momoo, N. Miyanaga, T. Hiromoto, and K. Tsuchida, *Appl. Phys. A Mater. Sci. Process.* 112, 173 (2013).
- [31] R. S. Wagner and W. C. Ellis, *Appl. Phys. Lett.* 4, 89 (1964).
- [32] Y. Nakata and N. Miyanaga, *Appl. Phys. A Mater. Sci. Process.* 98, 401 (2010).
- [33] Y. Nakata, T. Okada and M. Maeda, *Japanese J. Appl. Physics, Part 2 Lett.* 42, 379 (2003).
- [34] K. Kawamura, M. Hirano, T. Kamiya, T. Daizyu, T. Kamiya, et al. *Appl. Phys. Lett.* 84, 311 (2004).
- [35] T. Kondo, S. Matsuo, S. Juodkakis, V. Mizeikis and H. Misawa, *Appl. Phys. Lett.* 82, 2758 (2003).
- [36] S. Juodkakis, V. Mizeikis and H. Misawa, *J. Appl. Phys.* 106, 1 (2009).

**Yoshiki Nakata**

Institute of Laser Engineering, Osaka
University, 2-6 Yamadaoka, Suita, Osaka
565-0871, Japan
nakata-y@ile.osaka-u.ac.jp

Yoshiki Nakata received his MS and PhD from Kyushu University, Fukuoka, Japan, in 1994 and 1996, respectively. In 1996 he joined the Graduate school of Information Science and Electrical Engineering, Kyushu University, Fukuoka, Japan, as a research associate. In 2006 he joined the Institute of Laser Engineering (ILE), Osaka University, Osaka, Japan, as an Associate Professor. His research interests are material processing by ultrashort laser, laser spectroscopy, fabrication of nanomaterials and their applications in optoelectronics, peta-watt laser project in ILE. He is a recipient of the Laser Society of Japan (LSJ) award for distinguished achievements in research (2011), LSJ award for research encouragement (2005), the 4th Funai information Technology Incentive Award, etc. He is a member of the Japan Society of Applied Physics (JSAP), the Institute of Electrical Engineering of Japan (IEEJ), LSJ, and the International Society for Optics and Photonics (SPIE).